Time-dependent multimode transport through quantum wires with spin-orbit interaction: Floquet scattering matrix approach

B. H. Wu and J. C. Cao

State Key Laboratory of Functional Materials for Informatics, Shanghai Institute of Microsystem and Information Technology, Chinese Academy of Sciences, 865 Changning Road, Shanghai 200050, People's Republic of China

(Received 13 March 2006; published 13 June 2006)

We investigate the ballistic spin transport in a multimode quantum wire with strong Rashba spin-orbit coupling and an oscillating potential. A spin-resolved Floquet scattering matrix and Floquet spin density matrix formalism is employed to study the transport properties, such as conductance and spin polarizations, of the device. Due to the strong Rashba coupling-induced drastic change of the dispersion relation, there are quasibound states formed beneath the bottom of each transverse mode. Interference between electrons through propagating modes and via the quasibound states will give a complex structure in the transport properties. By using an oscillating potential, the incident electrons can be trapped by or escape from the quasibound states via photon emission or absorption. As a result, asymmetric Fano line shapes can be found in our numerical results due to this photon-assisted interference. The properties of the mesoscopic device to retain the spin coherence of the injected spin states are also analyzed. When only one propagating mode is permitted, the spin coherence is well retained at static transport. However, when an oscillating potential is turned on, we found that the spin coherence, even when only one propagating mode is permitted, will be reduced. This is due to the existence of infinite Floquet states when the ac field is turned on. This mechanism of losing spin coherence should be taken into account in the design and operation of the mesoscopic spintronics devices with an ac field.

DOI: 10.1103/PhysRevB.73.245412 PACS number(s): 73.23.Ad, 71.70.Ej, 72.10.−d, 72.25.Dc

I. INTRODUCTION

Recently, much interest has been devoted to the manipulation of the electron spin degree of freedom for applications in spintronics.[1,2] The electric tunable Rashba spin-orbit coupling in two-dimensional electron gas (2DEG) due to the lack of structural inversion symmetry has inspired various proposals for nonmagnetic spintronics devices, such as spin cells, spin modulators, and spin detectors. One prominent paradigmatic spintronics device is the spin field-effect transistor proposed by Datta and Das.[3] In the Datta-Das transistor, a spin-polarized current is injected from a ferromagnetic contact and the electron spin will be coherently modulated by changing the strength of Rashba spin-orbit coupling via an electric gate. Therefore, two fundamental challenges in the Datta-Das transistor are effective spin injection and coherent spin manipulation. In the original proposal of Datta and Das, a perfect spin modulation was expected in a clean single-mode quantum wire with tunable Rashba spin-orbit coupling. However, it is not easy for nanotechniques on the cutting edge to have a quantum wire narrow enough to accommodate only one transverse mode. For example, to achieve single-mode operation, the quantum wire should have a width of the order 10 nm. Therefore, the multimode effects must be taken into account. The intermode mixing has been proven to play an important role in modulating the spin precession in the Datta-Das transistor.[4] When the Rashba coupling strength is strong and the influence of the interaction between different transverse modes is taken into account, it has been found that the modulation of spin-dependent conductance will deviate from the sinusoidal curve as expected in a single-mode model. On the other hand, when electrons are passing through a multimode quantum wire, the spin states in a different mode will be entangled. Therefore, the multimode transport will lead to the decay of the spin coherence of the injected current.[5] A reexamination of the multimode transport through the Datta-Das transistor has recently been undertaken via the scattering matrix method[6] or the Green function technique.[4]

Meanwhile, an active topic on the time-dependent mesoscopic transport has attracted much attention. A lot of interesting time-dependent phenomena have been theoretically investigated and experimentally identified for the spinless transport. We mention only microwave-induced zero resistance,[7–9] photon-assisted transport,[10–12] and absolute negative conductance.[13,14] It is thus intriguing to explore the spin-dependent phenomena due to the interplay of the spin-orbit interaction and an oscillating electric field. Several proposals for the spintronics have been put forward by modulating the shape of the quantum dot,[15] the spatial potential,[16,17] or the strength of the Rashba coupling[18] via a time-dependent gate. More recently, it was found that an application of the terahertz electric field can induce the spin polarization in 2DEG.[19] However, the influence of the multimode on the time-dependent transport has not yet been fully investigated in previous studies. The motivation of the present paper is thus to study the spin-dependent time-modulated multimode transport.

In this paper, we present a multimode Floquet scattering matrix formalism to exactly study the spin-dependent time-modulated multimode transport in a quasi-one-dimensional quantum wire with Rashba spin-orbit coupling. For time-modulated single-mode transport, the Floquet scattering matrix formalism has already been developed to study the spinless dynamics properties of mesoscopic systems.[20,21] Recently, a static multimode scattering matrix method has been developed to study spin-dependent transport, including the influence of the interactions in different transverse

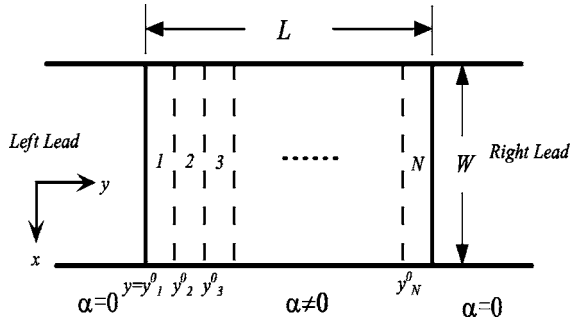

FIG. 1. Schematic plot of the model device. Strong Rashba spin-orbit coupling exists in the central region of length L and width W. This device is connected to the left and right semi-infinite ideal leads. The central part is divided into N stripes in the y direction for the sake of numerical simulation.

modes.[6] In what follows, we generalize the static multimode scattering matrix formalism to the time-dependent situation with the help of Floquet theory. After obtaining the Floquet scattering matrix, the coherence and modulation of spin polarization can be readily characterized by the Floquet spin density matrix formalism. In our model, we only consider a quantum wire with the Rashba effect at zero temperature. A generalization of the present formalism to the case of spin-dependent transport through a mesoscopic device with complex structure and not only the Rashba but also the Dresselhaus effect at nonzero temperature is straightforward.

The paper is organized as follows. In Sec. II, we present details on the spin-resolved multimode Floquet scattering matrix formalism and the Floquet spin density matrix. In Sec. III, the formalism presented in Sec. II is employed to investigate the spin transport properties in a quantum wire. Numerical results on the spin-resolved conductance and spin polarizations are presented and discussed, with or without an ac field. Finally, the main results of this work are concluded and summarized in Sec. IV.

II. MODEL AND FORMALISM

We consider the spin transport in a clean quasi-one-dimensional wire as depicted in Fig. 1. This quantum wire can be formed by applying a confining potential of the split-gate technique to a 2DEG in an asymmetric narrow-gap semiconductor quantum well. Due to the inversion asymmetry of the potential that confines the 2DEG, the spin degeneracy of the 2DEG is lifted by the Rashba spin-orbit coupling effect, which entangles the electron spin with its momentum. This quantum wire is lying in the x-y plane. We assume electrons can transport ballistically in the y direction. The width of the quantum wire is W. It consists of a central part of length L with a spatial variable Rashba spin-orbit coupling, which can be tuned by an external gates. This central part is connected to two semi-infinite leads, where the spin-orbit coupling is absent. In the following, we use a single-electron model where the electron-electron interactions are neglected. In addition, the temperature is assumed to be zero. The electron-phonon interactions can be neglected too. The effective mass Hamiltonian of the static system can therefore be written as

$$H_0 = \frac{\boldsymbol{p}^2}{2m^*} + U(\boldsymbol{r}) + V(x) + \frac{1}{2\hbar}[\alpha(\boldsymbol{r})(\boldsymbol{\sigma}\times\boldsymbol{p}) + (\boldsymbol{\sigma}\times\boldsymbol{p})\alpha(\boldsymbol{r})]_z, \tag{1}$$

where α represents the Rashba spin-orbit coupling strength, $\boldsymbol{\sigma}$ denotes the Pauli matrix vector, m^* is the effective mass, and $V(x)$ is the confining potential. $U(\boldsymbol{r})$ describes a general potential profile in the conductor. Since the spatial variation Rashba spin-orbit coupling contains the momentum operator, Eq. (1) has to be symmetrized to guarantee the Hermitian of the Hamiltonian.

We are interested in the case in which the device is modulated by a time-periodic potential. Solution of the Schrödinger equation will then be complicated by introducing a time-dependent field. Because the total Hamiltonian is time-dependent, the system has no stationary eigenstates. However, the symmetry of the Hamiltonian under discrete time translations, $t \to t+T$, where T is the period of the perturbation, enables the use of the Floquet theorem. In the following, we generalize the scattering matrix formalism in Ref. 6 to investigate the spin transport in an ac driven device with the help of the Floquet theorem[11,22] and Floquet spin density matrix formalism.[5]

As a first step, we divide the central part with Rashba spin-orbit coupling into N transverse stripes along the y direction, in line with Refs. 23 and 24. The width of each stripe is narrow enough so that we can take the Rashba term and the potential U as y-independent. Since the potentials in stripe j vary just in the transverse x direction, the solution of the Schrödinger equation in the stripe can be decomposed into the transverse part and the longitudinal part. Obviously, the longitudinal part is merely in the traveling (propagating or decaying) wave form. A set of complete and orthogonal eigenfunctions and their corresponding eigenenergies in the transverse x direction can be established from a one-dimensional Schrödinger equation in each stripe. We denote these transverse eigenfunctions in stripe j as $\varphi^j_{n,\sigma}(x)$. They are determined by

$$\left[-\frac{\hbar^2}{2m^*}\frac{d^2}{dy^2} + U^j(x) + V^j(x)\right]\varphi^j_{n,\sigma}(x) = E^j_n\varphi^j_{n,\sigma}(x), \tag{2}$$

where n is the eigenstate index and $\sigma = \uparrow, \downarrow$ stands for spin up or spin down in the z direction. Since the confining potential is spin-independent, these transverse eigenstates are spin degenerate. $U^j(x)$ and $V^j(x)$ are the potentials chosen to be the y coordinate at the center of the jth stripe.

Next, we introduce a time-dependent field to modulate the spintronics device. We assume only the central part is modulated by a monochromatic field with frequency ω. The Hamiltonian for the ac part is $H_{\rm ac} = V_{\rm ac}(\boldsymbol{r})\cos(\omega t)$, where $V_{\rm ac}$ is the intensity of the oscillating potential. The total Hamiltonian then reads $H = H_0 + H_{\rm ac}$. Since H is periodic in time, according to the Floquet theorem, solution of this time-periodic Schrödinger equation can be converted into a time-independent eigenvalue problem in a composed Hilbert space $\boldsymbol{R}\otimes\boldsymbol{T}$, where $\boldsymbol{R}$ is the space of functions in real space

and $\boldsymbol{T}$ is the space of periodic functions with period of the external ac field. We choose a suitable Floquet state in the composed Hilbert space in stripe j as

$$\phi^j_{n,m,\sigma} = e^{-im\omega t}\varphi^j_{n,\sigma}(\boldsymbol{r}). \tag{3}$$

The wave function for an electron with energy E can be expanded in the complete basis of the Floquet eigenstates given above. It should take the form

$$\Phi^j = e^{-iEt}e^{iky}\sum_{n,m} c^j_{n,m,\sigma}\phi^j_{n,m,\sigma}, \tag{4}$$

where k is the wave number in the y direction and $c^j_{n,m,\sigma}$ is the expanding coefficients for the given longitudinal eigenwave number k. Since each Floquet state can be occupied by only one electron due to the Pauli principle, the wave function Φ^j must be normalized as

$$\langle\langle \Phi^j|\Phi^j\rangle\rangle = \frac{1}{T}\int_0^T dt\int_{\boldsymbol{r}} d\boldsymbol{r}|\Phi^j|^2 = 1. \tag{5}$$

Here, we have used the notation $\langle\langle\cdots\rangle\rangle = \frac{1}{T}\int_0^T dt\langle\cdots\rangle$ and $T = 2\pi/\omega$ is the period time.

For a given energy E, we insert the wave function Eq. (4) into the time-dependent Schrödinger equation defined by the total Hamiltonian at stripe j,

$$i\hbar\frac{\partial}{\partial t}\Phi^j = H\Phi^j. \tag{6}$$

To find all the eigenwave numbers k and the corresponding coefficients, we use the technique developed in previous studies.[6,23,25] By introducing auxiliary coefficients $d^j_{n,m,\sigma} = kc^j_{n,m,\sigma}$ and notations $\boldsymbol{\mathcal{C}}^j = (\cdots c^j_{n,m,\sigma}\cdots)^T$, $\boldsymbol{\mathcal{D}}^j = k\boldsymbol{\mathcal{C}}^j$, and $\mu = \hbar^2/2m^*$, where $(\cdots)^T$ stands for the vector transpose, Eq. (6) can lead to the following secular equation:

$$\begin{pmatrix} 0 & 1 \\ \boldsymbol{\mathcal{S}} & \boldsymbol{\mathcal{T}} \end{pmatrix}\begin{pmatrix} \boldsymbol{\mathcal{C}} \\ \boldsymbol{\mathcal{D}} \end{pmatrix} = k\begin{pmatrix} \boldsymbol{\mathcal{C}} \\ \boldsymbol{\mathcal{D}} \end{pmatrix}. \tag{7}$$

Details of the derivation of this equations can be found in the Appendix.

For a given energy E, the above secular equation gives a set of eigenwave numbers, k^j_β. Their corresponding eigenvectors contain the expanding coefficients, $c^{\beta,j}_{n,m,\sigma}$. These coefficient vectors must be normalized according to Eq. (5). The transport properties of the device are determined by these wave numbers and their corresponding velocity. Due to the presence of the Rashba spin-orbit coupling, there is a shift in the dispersion relation. The sign of the velocity will not be identified with that of the corresponding eigenwave numbers. A proper determination of the sign of the velocities is one of the key points in constructing the Floquet scattering matrix formalism. The velocity along the y direction of each eigenwave number has to be determined from the equation of motion by the Hamiltonian. The velocity operator in the system is given by

TABLE I. Classification of the eigenmodes according to the value of wave number k and the corresponding velocity v.

	I	II
k_β: real	$v_\beta > 0$; right-propagating mode	$v_\beta < 0$; left-propagating mode
k_β: complex	$\mathrm{Im}(k_\beta) > 0$; right-decaying mode	$\mathrm{Im}(k_\beta) < 0$; left-decaying mode

$$\hat{v}_y = \frac{i}{\hbar}[H,y] = \frac{p_y}{m^*} + \frac{\alpha(\boldsymbol{r})}{\hbar}\sigma_x. \tag{8}$$

The expectation value of the velocity operator for a given k^j_β is given by

$$v^j_\beta = \sum_{\substack{n,m,\sigma \\ n',m',\sigma'}} (c^{\beta,j}_{n,m,\sigma})^* \times\left\langle \varphi^j_{n,\sigma}\left|\frac{\hbar k_\beta}{m^*} + \frac{\alpha(\boldsymbol{r})}{\hbar}\sigma_x\right|\varphi^j_{n',\sigma'}\right\rangle c^{\beta,j}_{n',m',\sigma'}\delta_{m,m'}. \tag{9}$$

For the purpose of constructing the scattering matrix, the set of solutions of Eq. (7) can be divided into two subsets. The first subset comprises right-going waves: the right-propagating or right-decaying modes. The corresponding eigenvalues are denoted by $k^j_{I_\beta}$. The second subset comprises left-going waves: the left-propagating or left-decaying modes. The corresponding eigenvalues are denoted by $k^j_{II_\beta}$. The mode property for a given wave number k^j_β is determined by the value of the wave number k^j_β and its corresponding velocity value v^j_β. For propagating modes, the eigenwave numbers k_β are real numbers. If the corresponding velocity is greater than zero, it is the right-propagating mode. Otherwise, it is the left-propagating mode. For evanescent modes, the corresponding eigenwave numbers are complex. The imaginary part of the eigenwave number will be positive for the right-decaying mode or negative for the left-decaying mode, respectively. It can be shown that the propagating states and evanescent modes always come in pairs, i.e., for every right-propagating or evanescent mode there is a left-propagating or evanescent mode. The classification of the wave modes is briefly summarized in Table I.

Now we can write down the eigenmodes in stripe j in terms of the Floquet eigenstates as

$$\Phi^j_\beta = \sum_{n,m,\sigma} c^{\beta,j}_{n,m,\sigma}e^{ik^j_\beta(y-y^0_j)}e^{-im\omega t}\varphi_{n,\sigma}, \tag{10}$$

where y^0_j is the reference coordinate along the y direction for the jth stripe. The wave function in stripe j can then be expressed as a linear combination of the obtained eigenmodes,

$$\Psi^j = e^{-iEt/\hbar}\left(\sum_{I_\beta} a^j_{I_\beta}\Phi^j_{I_\beta} + \sum_{II_\beta} a^j_{II_\beta}\Phi^j_{II_\beta}\right). \tag{11}$$

The set of unknown coefficients $\{a^j_{I_\beta}\}$ and $\{a^j_{II_\beta}\}$ in stripe j can be obtained by connecting two adjacent stripes via proper boundary conditions. The continuity requirements on

the electron wave function and flux at the interface between stripe j and stripe $j+1$ are written as

$$|\Psi^j\rangle_{y=y^0_{j+1}} = |\Psi^{j+1}\rangle_{y=y^0_{j+1}}, \tag{12}$$

$$\hat{v}^j_y|\Psi^j\rangle_{y=y^0_{j+1}} = \hat{v}^{j+1}_y|\Psi^{j+1}\rangle_{y=y^0_{j+1}}. \tag{13}$$

These equations lead to a set of linear equations containing the unknown coefficients in two adjacent stripes. A transfer matrix can then be constructed to connect coefficients in the stripe j and that in the stripe $(j+1)$,

$$\begin{pmatrix} \boldsymbol{A}^j_I \\ \boldsymbol{A}^j_{II} \end{pmatrix} = \boldsymbol{M}(j,j+1)\begin{pmatrix} \boldsymbol{A}^{j+1}_I \\ \boldsymbol{A}^{j+1}_{II} \end{pmatrix}, \tag{14}$$

where $\boldsymbol{A}^j_I$ and $\boldsymbol{A}^j_{II}$ are coefficient vectors containing $\{a^j_{I_\beta}\}$ and $\{a^j_{II_\beta}\}$, respectively. It can be shown that the transfer matrix $\boldsymbol{M}(j,j+1)$ can be written as

$$\boldsymbol{M}(j,j+1) = \begin{pmatrix} \boldsymbol{\Gamma}^j_I & 0 \\ 0 & \boldsymbol{\Gamma}^j_{II} \end{pmatrix}^{-1}\begin{pmatrix} \boldsymbol{P}^j_I & \boldsymbol{P}^j_{II} \\ \boldsymbol{Q}^j_I & \boldsymbol{Q}^j_{II} \end{pmatrix}^{-1}\begin{pmatrix} \boldsymbol{P}^{j+1}_I & \boldsymbol{P}^{j+1}_{II} \\ \boldsymbol{Q}^{j+1}_I & \boldsymbol{Q}^{j+1}_{II} \end{pmatrix},$$

where

$$(\boldsymbol{\Gamma}^j_I)_{I_\beta I_\beta} = e^{ik^j_{I_\beta} l^j},$$

$$(\boldsymbol{\Gamma}^j_{II})_{II_\beta, II_\beta} = e^{ik^j_{II_\beta} l^j},$$

$$(\boldsymbol{P}^j_I)_{n,m,\sigma;I_\beta} = c^{I_\beta,j}_{n,m,\sigma},$$

$$(\boldsymbol{P}^j_{II})_{n,m,\sigma;II_\beta} = c^{II_\beta,j}_{n,m,\sigma},$$

$$(\boldsymbol{Q}^j_I)_{n,m,\sigma;I_\beta} = \sum_{n'}\left[\frac{\hbar k^j_{I_\beta}}{m^*}c^{I_\beta,j}_{n',m,\sigma}\delta_{nn'} + \frac{\alpha_{nn'}}{\hbar}c^{I_\beta,j}_{n',m,-\sigma}\right],$$

$$(\boldsymbol{Q}^j_{II})_{n,m,\sigma;II_\beta} = \sum_{n'}\left[\frac{\hbar k^j_{II_\beta}}{m^*}c^{II_\beta,j}_{n',m,\sigma}\delta_{nn'} + \frac{\alpha_{nn'}}{\hbar}c^{II_\beta,j}_{n',m,-\sigma}\right]. \tag{15}$$

The total transfer matrix connecting the expansion coefficients of the electron wave functions in the left and right leads can be found from matrix multiplication of the individual matrices connecting adjacent stripes as

$$\boldsymbol{M}(L,R) = \boldsymbol{M}(L,1) \times \prod_{j=1}^{N-1}\boldsymbol{M}(j,j+1) \times \boldsymbol{M}(N,R), \tag{16}$$

where $\boldsymbol{M}(L,1)$ and $\boldsymbol{M}(N,R)$ are the two transfer matrices that couple the wave function in the conductor and that in the two leads. All the transport properties can be derived from the information of the transfer matrix. However, it is well know that the transfer-matrix method suffers numerical instability due to the exponential terms in the formalism. This shortcoming can be overcame by converting the transfer matrix to the corresponding scattering matrix[23,26] which connects the outgoing waves from the conductor with the incoming waves as

$$\begin{pmatrix} \boldsymbol{A}^R_I \\ \boldsymbol{A}^L_{II} \end{pmatrix} = \boldsymbol{S}(L,R)\begin{pmatrix} \boldsymbol{A}^L_I \\ \boldsymbol{A}^R_{II} \end{pmatrix} = \begin{pmatrix} \boldsymbol{S}_{11}(L,R) & \boldsymbol{S}_{12}(L,R) \\ \boldsymbol{S}_{21}(L,R) & \boldsymbol{S}_{22}(L,R) \end{pmatrix}\begin{pmatrix} \boldsymbol{A}^L_I \\ \boldsymbol{A}^R_{II} \end{pmatrix}. \tag{17}$$

We refer to Refs. 23 and 26 for a detailed description on the procedure of converting the transfer matrix into the desired scattering matrix.

We are interested in the spin transport properties at zero temperature. A transmission matrix $\mathcal{T}$ can be established with the help of the scattering matrix $\boldsymbol{S}_{11}(L,R)$ which connects the incoming right-propagating waves in the left lead and the outgoing right-propagating modes in the right lead. The matrix element $t_{n,m,\sigma;n',m',\sigma'}$ in $\mathcal{T}$ is the transmission amplitude and can be given by

$$t_{n,m,\sigma;n',m',\sigma'} = \begin{cases} \sqrt{\dfrac{k_{n,m,\sigma}}{k_{n',m',\sigma'}}}\boldsymbol{S}_{11}(L,R)_{n,m,\sigma;n',m',\sigma'}, & E > \max(E_n - m\hbar\omega, E_{n'} - m'\hbar\omega) \\ 0 & \text{otherwise}. \end{cases} \tag{18}$$

The condition $E > \max(E_n - m\hbar\omega, E_{n'} - m'\hbar\omega)$ guarantees that both the incoming and outgoing modes are propagating modes. The wave numbers in the propagating modes are real and determined by the relation $k_{n,m,\sigma} = \sqrt{2m^*(E - E_n + m\hbar\omega)}/\hbar$. Elements of the transmission matrix that describe the injection or collection of electrons in the evanescent modes are set zero. Since the terms in $\boldsymbol{S}_{11}$ describe only the transmitted wave amplitude, the factor $\sqrt{\frac{k_{n,m,\sigma}}{k_{n',m',\sigma'}}}$ has to be used to satisfy the prerequisite of the current conservation and make the Floquet scattering matrix unitary, where (n,m,σ) and (n',m',σ') are indices in the perfect right lead and left lead, respectively. The matrix element $t_{n,m,\sigma;n',m',\sigma'}$ has a straightforward physical meaning. It describes the probability of an electron appearing at the $|n,m,\sigma\rangle$ mode in the right lead after it was injected to the $|n',m',\sigma'\rangle$ mode from the left lead.

From the transmission matrix, we can calculate the (spin-resolved) conductance of the mesoscopic device. Let us consider electrons with spin state σ that are incident from the left with a fixed Fermi energy E. Only the elements $\boldsymbol{A}^L_I(n,0,\sigma) = 1$ are nonzero, where n is the index of permitted

propagating modes and satisfies $E > E_n$. When the electrons are transported through the device, electrons can be scattered into different propagating Floquet states in the right lead involving multiphoton emission or absorption. The spin-resolved partial conductance can be found from the Landauer-Büttiker formula as

$$G^{\sigma,\sigma'} = \frac{e^2}{h} \sum_{n,m;n'} |t_{n,m,\sigma;n',0,\sigma'}|^2. \tag{19}$$

$G^{\sigma,\sigma'}$ describes transmitted electron flux at the σ state in the right lead when only spin σ' electrons at Fermi energy E are injected from the left lead.

In determining the spin-resolved partial conductance in Eq. (19), only the amplitude of the transmission matrix element is needed. However, the output electron states are relevant not only to the amplitude but also to the phase of the transmission matrix elements. Suppose partially polarized currents are injected from the left lead. The spins are in the mixed quantum states

$$\hat{\rho}_i = n_\uparrow |\uparrow\rangle\langle\uparrow| + n_\downarrow |\downarrow\rangle\langle\downarrow|. \tag{20}$$

For the fully σ-spin-polarized injection, one has $n_\sigma = 1$ and $n_{\bar{\sigma}} = 0$. On the other hand, for the unpolarized injection, one has $n_\downarrow = n_\uparrow = \frac{1}{2}$. For the transmitted electron flux, the spin density matrix[5] can be written, in terms of the transmission matrix, as

$$\hat{\rho}_o = \frac{1}{n_\uparrow |t_{\beta\uparrow;\beta'\uparrow}|^2 + n_\downarrow |t_{\beta\uparrow;\beta'\downarrow}|^2 + n_\uparrow |t_{\beta\downarrow;\beta'\uparrow}|^2 + n_\downarrow |t_{\beta\downarrow;\beta'\downarrow}|^2} \times \sum_{\beta\beta'} \begin{pmatrix} n_\uparrow |t_{\beta\uparrow;\beta'\uparrow}|^2 + n_\downarrow |t_{\beta\uparrow;\beta'\downarrow}|^2 & n_\uparrow t_{\beta\uparrow;\beta'\uparrow} t^*_{\beta\downarrow;\beta'\uparrow} + n_\downarrow t_{\beta\uparrow;\beta'\downarrow} t^*_{\beta\downarrow;\beta'\downarrow} \\ n_\uparrow t^*_{\beta\uparrow;\beta'\uparrow} t_{\beta\downarrow;\beta'\uparrow} + n_\downarrow t^*_{\beta\uparrow;\beta'\downarrow} t_{\beta\downarrow;\beta'\downarrow} & n_\uparrow |t_{\beta\downarrow;\beta'\uparrow}|^2 + n_\downarrow |t_{\beta\downarrow;\beta'\downarrow}|^2 \end{pmatrix}, \tag{21}$$

where we have used the notation $\beta = (n,m)$ and $\beta' = (n',0)$ for simplicity. The incident electrons are in the zero-photon Floquet states. Therefore, we have set $m' = 0$ in β'. To investigate the spin transport, we need all the information on spin polarization in different directions. The spin density matrix formalism enables us to have a direct algorithm to obtain the explicit formulas for this information. With the help of the spin density matrix, the output flux spin polarization can be easily obtained from

$$P_\alpha = \mathrm{Tr}\{\sigma_\alpha \hat{\rho}_o\}, \tag{22}$$

where $\alpha = x, y, z$ and σ_α are the Pauli matrices. The coherence of the spin states can be evaluated from the magnitude of the spin-polarized vector,

$$P = \sqrt{P_x^2 + P_y^2 + P_z^2}. \tag{23}$$

$P = 1$ for fully spin polarized current while $P < 1$ for partially polarized current. The decay of the spin coherence can be characterized by measuring the reduction of P.

III. NUMERICAL RESULTS AND DISCUSSION

In this section, we apply the formalism presented above to investigate the spin transport with the influence of an ac field. Numerical results on the conductance and the spin polarization are presented to explore the time-modulated effects on the spin transport in the multimode quantum wire. In our numerical calculation, material parameters are chosen to be consistent with the InGaAs-InAlAs based narrow-gap heterostructures. The electron effective mass $m^* = 0.042 m_0$, where m_0 is the free-electron mass. The Rashba coupling strength in the central region is $\alpha = 4 \times 10^{-11}$ eV m.[27,28] The geometry parameters of the conductor are width $W = 100$ nm and length $L = 250$ nm. The potential in the conductor U is assumed to be zero for simplicity. We choose a hard-wall confinement potential in the transverse direction as

$$V(x) = \begin{cases} 0, & |x| \le W/2 \\ \infty, & |x| > W/2 \end{cases}. \tag{24}$$

The transverse eigenfunctions are then given by

$$\varphi_{n,\sigma}(x) = \begin{cases} \sqrt{\frac{2}{W}} \sin\left[\frac{n\pi}{W}\left(x + \frac{W}{2}\right)\right], & |x| \le \frac{W}{2} \\ 0, & |x| > \frac{W}{2}, \end{cases}$$

$$n = 1, 2, \ldots .$$

The corresponding eigenenergies are simply given by

$$E_n = \frac{\hbar^2}{2m^*}\left(\frac{n\pi}{W}\right)^2.$$

For the parameters chosen above, the first transverse mode energy is approximately given by $E_1 = 0.89$ meV. We will use E_1 as an energy unit in the following discussions. The nth transverse mode energy is $n^2 E_1$. In the calculation, one has to truncate the infinite number of Floquet states used in the above formalism. In the actual numerical results, the number of the transverse modes and the minimum number of photon sidebands that need to be included are determined on the convergence of the desired transport quantities. For a higher Fermi energy or a higher ac field strength, the numerical calculations will be more CPU consuming since a larger number of the transverse modes and Floquet states should be included.

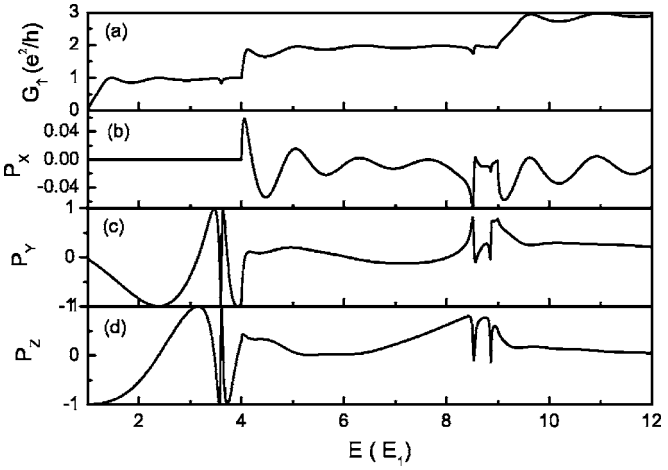

FIG. 2. Conductance $G_\uparrow = G_{\uparrow\uparrow} + G_{\downarrow\uparrow}$ for up-spin injection and spin polarizations in the x, y, and z directions at vanishing oscillating potential as a function of the Fermi energy E (in units of the energy of the first transverse mode energy). The Rashba strength is $\alpha = 4 \times 10^{-11}$ eV m. The width of the quantum wire is $W = 100$ nm. The length of the central device is $L = 250$ nm. Only spin-up electrons are injected into the device.

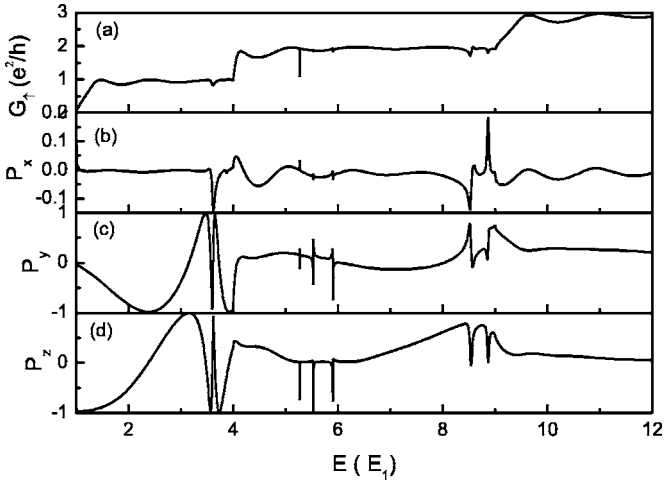

FIG. 3. Conductance $G_\uparrow = G_{\uparrow\uparrow} + G_{\downarrow\uparrow}$ for up-spin injection and spin polarizations in the x, y, and z directions with the influence of an oscillating potential as a function of the Fermi energy E (in units of the energy of the first transverse mode energy). The model parameters are the same as those given in Fig. 2 except that the oscillating frequency $\hbar\omega = 5E_1$ and the intensity of the oscillating field $V_{ac} = 1\ E_1$ are used in the calculations.

A. Quasibound states induced transmission resonance

We are interested in the features caused by the interplay of strong Rashba spin-orbit coupling and the external ac field to the quantum wire. As a first step, for the sake of comparison, we apply the formalism presented above to a static quantum wire with strong Rashba spin-orbit coupling ($\alpha = 4 \times 10^{-11}$ eV m). Obviously, when the ac field vanishes, the Floquet scattering matrix formalism is reduced to results presented in Ref. 6. Let us consider the situation in which only the spin-up electrons are injected from the left lead, i.e., $n_\uparrow = 1$ and $n_\downarrow = 0$. The strong Rashba spin-orbit coupling can lead to a drastic change in the dispersion relation of the transverse modes and therefore the transport properties of the quantum wire. The presence of strong Rashba spin-orbit coupling in the device will contribute to the system an effective spin-dependent potential. Therefore, the transverse mode number and longitudinal wave numbers in the ideal leads are no longer good ones in the central part. There will be quasibound states formed just beneath the transverse mode bottom.[6,29] Interference between electrons passing through the device with the Rashba term via propagating modes and those via the quasibound states can lead to asymmetric resonance dips in the spin-resolved conductance results. On the other hand, the strong Rashba coupling is expected to have a fundamental impact on the spin modulation due to the strong Rashba coupling-induced large mixing between different transverse modes.

Numerical results on the total conductance and spin polarizations in the x, y, and z direction as a function of the Fermi energy E (in units of the energy of the first transverse mode E_1) are displayed, respectively, in Fig. 2. In Fig. 2(a), the conductance results deviate from the perfect steplike conductance quantization in an ideal ballistic wire as predicted by the Landauer formula. The complex curve of conductance indicates the nontrivial intermode mixing as discussed in Ref. 6. One can identify sharp conductance dips at energies just beneath the bottom of each transverse mode where complicated transverse mode mixing is expected. Particularly, very fast spin polarization oscillations can be found around these energy levels as shown in Figs. 2(b)–2(d). Contrary to the predictions in the single-mode Datta-Das transistor model, the calculated spin polarizations P_x, P_y, and P_z displayed in Fig. 2 are all sensitive to the change of the Fermi energy. Especially, at energies near the transverse mode bottom, the output spin polarizations show drastic oscillations due to the interference effects as discussed above. This is different from the expectations at weak Rashba coupling,[3] where the outgoing polarization is almost independent of the Fermi energy.

Since the quasibound states induced asymmetric transmission resonance dips appears below the onset energy of the transverse mode and the propagating electrons must have energies higher than the first transverse mode eigenenergy, one cannot identify in Fig. 2 the transmission resonance dips due the quasibound states formed by the first transverse modes.[6] In the following, we show that by applying the ac field, we can identify the asymmetric transmission resonance line shapes caused by the formation of quasibound states near the first transverse mode bottom due to photon assisted transport.

In Fig. 3, we depict the conductance and the spin polarizations in different directions as a function of energy of incident electrons with the ac frequency of $\hbar\omega = 5E_1$ which is in the terahertz region. The intensity $V_{ac} = 1E_1$. All the other parameters are the same as those in Fig. 2. Comparing the conductance result in Fig. 3(a) with that of Fig. 2(a), one can find that three transmission resonances formed at energies around $E = 5.6E_1$. These transmission resonances show asymmetric Fano line shapes,[30] where sharp dips are followed by peaks. These resonances result from the transition and inter-

ference of electrons among Floquet states.[31] When the energy E of the incident electrons equals the summation of the quasibound states energy E_{QB} and one or more photons with the frequency of the external ac field,

$$E_{\mathrm{QB}} + m\hbar\,\omega = E, \quad m = \pm 1, \pm 2, \ldots, \tag{25}$$

where the $m>0$ and $m<0$ indicate, respectively, the absorption and emission of $|m|$ photons, the electrons are able to transit to or escape from the quasibound states via photon-assisted transport. Electrons with energy around $E=5.6E_1$ can emit one photon and drop to the quasibound states formed beneath the first transverse mode. In a similar way, electrons in the quasibound states can also absorb m photons and jump to a Floquet state. The transmission resonances in Fig. 3 around $5.5E_1$ are direct examples of this photon-assisted Fano interference. This photon-assisted Fano interference also leaves fingerprints in the spin polarizations results, as can be seen from Figs. 3(b)–3(d). Very sharp asymmetric line shapes in the results of spin polarization appear at energies where the interference takes place. Our numerical results show that by tuning the external ac frequency, the positions of transmission Fano resonances will be shifted in accordance with Eq. (25). Therefore, Eq. (25) suggests an effective way to determine the position of the quasibound states via applying a high-frequency oscillating potential.

Despite the asymmetric resonance line shapes caused by trapping electrons to the quasibound states, one must note that electrons in the quasibound states can also escape via photon absorption or emission to a propagating channel. This mechanism will lead to drastic changes of the transport property at energy levels of the quasibound states. As an example, this effect can be seen more clearly by comparing P_x in Fig. 2(b) and 3(b). Very large polarizations in the x directions can be induced near the bottoms of the second and third transverse modes where quasibound states exist if we turn on the ac field. Note that the scales of P_x in Fig. 2(b) and 3(b) are different. Since these drastic changes take place at the quasibound state levels, they will not shift with the ac frequency. This property was also verified in our numerical results, which are not presented here.

Therefore, there are two types of drastic change to the transport properties due to an external ac field. For the asymmetric line shapes caused by trapping electrons to the quasibound states via photon emission or absorption, the positions of these line shapes are determined by Eq. (25) and therefore can be tuned by changing the frequency of the ac field. However, for the second type, the energy positions of the drastic change caused by pumping electrons out of the quasibound state will not shift by tuning the ac frequency.

B. Spin coherence in transport through the quantum wire

In spintronics, one key figure of merit is the coherence of the spin states. A lot of spintronics devices based on the microscopic spin-orbit couplings are proposed to utilize the ballistic transport to avoid such detrimental effects as disorder and maintain a good spin coherence. To quantify the degree of coherence of transported spin states in a mesoscopic device, the magnitude of the spin polarization vector P has to be evaluated.[5] In Figs. 4 and 5, we present the calculated magnitude of the spin polarization vector as a function of the Fermi energy without or with the ac field, respectively. The parameters used in the numerical calculations are the same as those in Figs. 2 and 3. Only spin-up electrons are injected from the left lead.

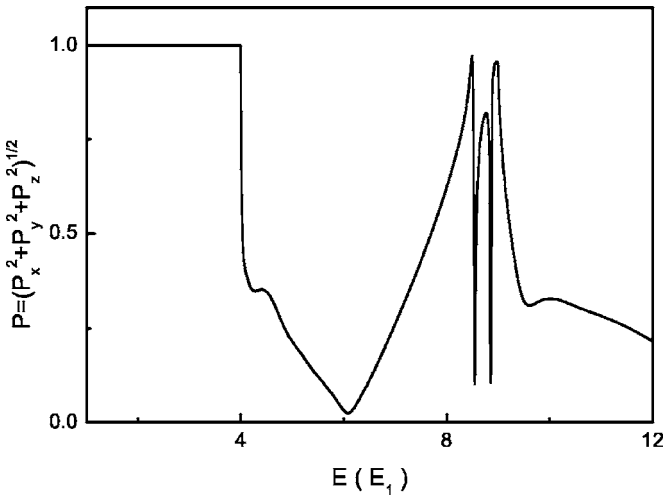

FIG. 4. Magnitude of the spin polarization vector P at vanishing oscillating field as a function of the electron Fermi energy E. The parameters are identical to those given in Fig. 2.

For the situations without ac field, the spin coherence has been numerically investigated and discussed in Ref. 5. In Fig. 4, we show the magnitude of the spin polarization vector as a function of the Fermi energy where the ac field vanishes. When only the first transverse mode is open, the spin state maintains its coherence ($P=1$) after passing through the quantum wire with strong Rashba coupling. This is due to the fact that if there is only one propagating mode in the lead, the outgoing electrons have to stay in the single transverse mode.[5] When the energy is high enough to include the second transverse mode, the spin polarization loss its purity

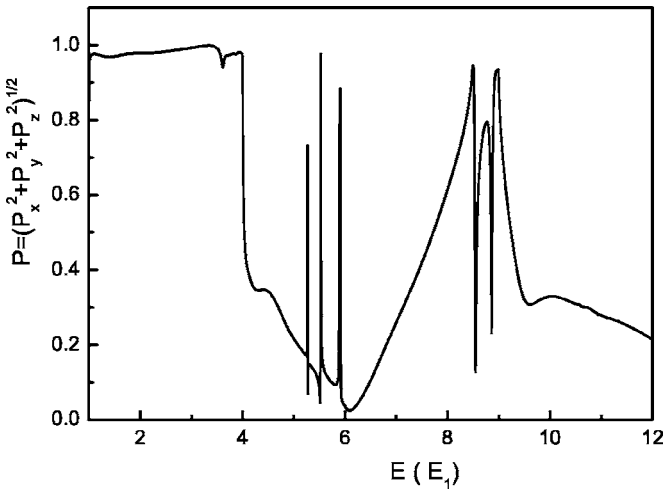

FIG. 5. Magnitude of the spin polarization vector P with the influence of an oscillating field as a function of the electron Fermi energy E. The parameters are the same as those given in Fig. 3.

and $P<1$. This loss of spin coherence can be ascribed to the entanglement of the spin states in different transverse modes due to the Rashba coupling-induced mode mixing effects. In the multimode transport, incident electrons with the same velocity can be scattered into different transverse modes and possess different speed and phase properties at the outgoing lead, resulting in the loss of spin coherence. This mechanism of the reduction of spin coherence has been proven to affect the operation of any multimode mesoscopic device,[5] regardless of whether the relation between the Rashba term and the Dresselhaus term or the device region is clear or not. When we increase the Fermi energy, P does not show a monotonic decrease. Especially, one can find rapid oscillations of P at energies around the quasibound state formed at the higher transverse mode bottom in Fig. 4.

In the above analysis, we note that the mixing between spin states in different transverse modes will lead to a drop of the purity of injected spin states. When we have an ac field, electrons can transport via a set of infinite Floquet channels. It is now interesting to ask whether these Floquet channels will lead to the loss of spin coherence in the absence of intermode mixing. It is important to study the spin coherence in the presence of an ac field since many spintronics proposals have relied on photon-assisted transport. In Fig. 5, we show that when the ac field is turned on, the magnitude of the spin polarization will be lowered regardless of the propagating mode number. This is not surprising since we have included a set of infinite Floquet states due to the existence of an ac field even in the case of single mode transport. When the electrons are injected with energies E lower than the second transverse modes, they can be scattered to the propagating modes in the right lead with energies of $E+m\hbar\omega$ via m-photon absorption and gain different velocity and phase properties. The Rashba term will entangle all these spin states in the Floquet states. Therefore, the spin polarization will lose its purity even if the electrons are only injected from the lowest transverse mode. By increasing the intensity of the ac field, a large reduction of the spin coherence occurs since a strong ac field inclines electrons to jump to the other Floquet states via photon absorption. Furthermore, at energies where the photon-assisted transition to the quasibound states occurs, the magnitude of the spin polarization vector shows a very sharp peak. This occurs because electrons at those energies satisfying Eq. (25) can easily be scattered to the quasibound states, which are not propagating modes and make no contribution to the transport. This effectively decreases the impact of mixing between different Floquet states and therefore increases spin purity P. This mechanism of losing spin purity must be taken into account in the design and operation of the mesoscopic spintronics devices with an ac field even if only one mode is included. One has to choose a proper ac frequency and intensity for spintronics to enable the photon-assisted transport and, at the time, retain the coherence of the incident spin states.

IV. CONCLUSION

In conclusion, we have presented a general spin-resolved Floquet scattering matrix formalism to investigate the spin transport properties in quantum wires with strong Rashba spin-orbit coupling. Due to the strong Rashba coupling-induced drastic change of the dispersion relation, there are quasibound states formed beneath the bottom of each transverse mode. Interference between electrons through propagating modes and via the quasibound states will give a complex structure in the transport properties. By using an oscillating potential, the incident electrons can be trapped by the quasibound states via photon emission or absorption. As a result, asymmetric Fano line shapes can be found in our numerical results due to the photon-assisted interference. The properties of the mesoscopic device to retain the spin coherence of the injected spin states are also analyzed. When the oscillating potential is turned on, the spin coherence will be reduced due to the set of infinite Floquet states, even when the Fermi energy is lower than the second transverse mode. This mechanism of losing spin coherence should be taken into account in the design and operation of the mesoscopic spintronics devices with an ac field.

ACKNOWLEDGMENTS

This work was supported by the National Science Foundation of China (Grants No. 60506018 and No. 60425415), the major project of the National Science Foundation of China (Grant No. 10390162), and the Shanghai Municipal Commission of Science and Technology (Grant No. 05XD14020).

APPENDIX A

In this appendix, we will explain the details in deriving Eq. (7). By inserting the wavefunction given in Eq. (4) and matching the left hand side and the right hand side of the Schrödinger equation (6), we can obtain

$$\left(E+m\hbar\omega-E_n^j-\frac{\hbar^2k^2}{2m^*}\right)c_{n,m,\sigma}^j = \sum_{n',\sigma'}\left(k\alpha_{nn'}^j+\sigma\eta_{nn'}^j+\frac{\sigma}{2}\chi_{nn'}^j\right)\times\delta^{\sigma,-\sigma'}c_{n',m,\sigma'}^j+\sum_{n'}U_{nn'}^j c_{n',m,\sigma}^j + \sum_{n'}\frac{V_{ac;nn'}^j}{2}(c_{n',m+1,\sigma}^j+c_{n',m-1,\sigma}^j), \tag{A1}$$

where we have used the following notations:

$$\eta_{nn'}^j=\left\langle\varphi_{n,\sigma}\left|\alpha^j(x)\frac{\partial}{\partial x}\right|\varphi_{n',\sigma}\right\rangle,$$

$$\chi_{nn'}^j=\left\langle\varphi_{n,\sigma}\left|\frac{\partial\alpha^j(x)}{\partial x}\right|\varphi_{n',\sigma}^j\right\rangle,$$

$$\alpha_{nn'}^j=\langle\varphi_{n,\sigma}|\alpha^j(x)|\varphi_{n',\sigma}\rangle,$$

$$U_{nn'}^j=\langle\varphi_{n,\sigma}|U^j(x)|\varphi_{n',\sigma}\rangle,$$

$$V^j_{ac;nn'} = \langle \varphi_{n,\sigma} | V^j_{ac}(x) | \varphi_{n',\sigma} \rangle. \quad \text{(A2)}$$

Equation (A1) defines a set of linear equations that couple the expanding coefficients of different index (n,m,σ). On the right hand side of Eq. (A1), the first term represents the intra- or intermode spin state mixing due to the Rashba spin-orbit coupling. The second term describes the mixing between different modes due to the spin-independent potential in the conductor region. The third term on the right hand side stands for the interaction between different Floquet states due to the external ac field. It is more useful to write Eq. (A1) into a matrix form. After some algebra, Eq. (A1) finally leads to the secular equation as Eq. (7), whose matrix elements are given by

$$\begin{aligned} S_{n,m,\sigma;n',m',\sigma'} = & \frac{1}{\mu}(E + m\hbar\,\omega - E_n)\delta_{n,n'}\delta_{m,m'}\delta_{\sigma,\sigma'} \\ & - U^j_{nn'}\delta_{m,m'}\delta_{\sigma,\sigma'} - \frac{1}{\mu}\sigma\eta^j_{n,n'}\delta_{m,m'}\delta_{\sigma,-\sigma'} \\ & - \frac{1}{\mu}\frac{\sigma}{2}\chi^j_{n,n'}\delta_{m,m'}\delta_{\sigma,-\sigma'} \\ & - \frac{1}{\mu}\frac{V^j_{ac;nn'}}{2}\delta_{\sigma,\sigma'}(\delta_{m,m'+1} + \delta_{m,m'-1}), \end{aligned} \quad \text{(A3)}$$

$$T_{n,m,\sigma;n',m',\sigma'} = -\frac{1}{\mu}\alpha^j_{n,n'}\delta_{m,m'}\delta_{\sigma,-\sigma'}. \quad \text{(A4)}$$

[1] I. Žutić, J. Fabian, and S. S. Das, Rev. Mod. Phys. **76**, 323 (2004).
[2] R. H. Silsbee, J. Phys.: Condens. Matter **16**, R179 (2004).
[3] S. Datta and B. Das, Appl. Phys. Lett. **56**, 665 (1990).
[4] F. Mireles and G. Kirczenow, Phys. Rev. B **64**, 024426 (2001).
[5] B. K. Nikolić and S. Souma, Phys. Rev. B **71**, 195328 (2005).
[6] L. Zhang, P. Brusheim, and H. Q. Xu, Phys. Rev. B **72**, 045347 (2005).
[7] R. G. Mani, J. H. Smet, K. von Klitzing, V. Narayanamurti, W. B. Johnson, and V. Umansky, Nature (London) **420**, 646 (2002).
[8] M. A. Zudov, R. R. Du, L. N. Pfeiffer, and K. W. West, Phys. Rev. Lett. **90**, 046807 (2003).
[9] A. C. Durst, S. Sachdev, N. Read, and S. M. Girvin, Phys. Rev. Lett. **91**, 086803 (2003).
[10] P. K. Tien and J. P. Gordon, Phys. Rev. **129**, 647 (1963).
[11] M. Grifoni and P. Hänggi, Phys. Rep. **304**, 229 (1998).
[12] G. Platero and R. Aguado, Phys. Rep. **395**, 1 (2004).
[13] B. J. Keay, S. Zeuner, S. J. Allen, K. D. Maranowski, A. C. Gossard, U. Bhattacharya, and M. J. W. Rodwell, Phys. Rev. Lett. **75**, 4102 (1995).
[14] S. Zeuner, B. J. Keay, S. J. Allen, K. D. Marnowski, A. C. Gossard, U. Bhattacharya, and M. J. W. Rodwell, Phys. Rev. B **53**, R1717 (1996).
[15] P. Sharma and P. W. Brouwer, Phys. Rev. Lett. **91**, 166801 (2003).
[16] M. Governale, F. Taddei, and R. Fazio, Phys. Rev. B **68**, 155324 (2003).
[17] P. Kleinert and V. V. Bryksin, Phys. Rev. B **72**, 153103 (2005).
[18] A. G. Mal'shukov, C. S. Tang, C. S. Chu, and K. A. Chao, Phys. Rev. B **68**, 233307 (2003).
[19] J. L. Cheng and M. W. Wu, Appl. Phys. Lett. **86**, 032107 (2005).
[20] W. Li and L. E. Reichl, Phys. Rev. B **60**, 15732 (1999).
[21] M. Moskalets and M. Büttiker, Phys. Rev. B **66**, 245321 (2002).
[22] J. H. Shirley, Phys. Rev. **138**, B979 (1965).
[23] H. Xu, Phys. Rev. B **50**, 8469 (1994).
[24] H. Xu, Phys. Rev. B **52**, 5803 (1995).
[25] H. Tamura and T. Ando, Phys. Rev. B **44**, 1792 (1991).
[26] David Yuk Kei Ko and J. C. Inkson, Phys. Rev. B **38**, 9945 (1988).
[27] D. Grundler, Phys. Rev. Lett. **84**, 6074 (2000).
[28] J. Nitta, T. Akazaki, H. Takayangi, and T. Enoki, Phys. Rev. Lett. **78**, 1335 (1997).
[29] I. A. Shelykh and N. G. Galkin, Phys. Rev. B **70**, 205328 (2004).
[30] U. Fano, Phys. Rev. **124**, 1866 (1961).
[31] W. Li and L. E. Reichl, Phys. Rev. B **62**, 8269 (2000).